ISSN 0915-633X

INTERNATIONAL ATOMIC ENERGY AGENCY

17th IAEA Fusion Energy Conference
Yokohama, Japan, 19 - 24 October 1998

IAEA-CN-69/OV4/5

NATIONAL INSTITUTE FOR FUSION SCIENCE

Confinement Physics Study in a Small Low-Aspect-Ratio Helical Device CHS

S. Okamura, K. Matsuoka, R. Akiyama, D.S. Darrow, A. Ejiri, A. Fujisawa, M. Fujiwara, M. Goto, K. Ida H. Idei, H. Iguchi, N. Inoue, M. Isobe, K. Itoh, S. Kado, K. Khlopenkov, T. Kondo, S. Kubo, A. Lazaros, S. Lee, G. Matsunaga, T. Minami, S. Morita, S. Murakami, N. Nakajima, N. Nikai, S. Nishimura, I. Nomura, S. Ohdachi, K. Ohkuni, M. Osakabe, R. Pavlichenko, B. Peterson, R. Sakamoto, H. Sanuki, M. Sasao, A. Shimizu, Y. Shirai, S. Sudo, S. Takagi, C. Takahashi, S. Takayama, M. Takechi, K. Tanaka, K. Toi, K. Yamazaki, Y. Yoshimura and T. Watari

(Received - Oct. 5. 1998)

NIFS-568 Oct. 1998

RESEARCH REPORT
NIFS Series

NAGOYA, JAPAN

CONFINEMENT PHYSICS STUDY IN A SMALL LOW-ASPECT-RATIO HELICAL DEVICE CHS

S. OKAMURA, K. MATSUOKA, R. AKIYAMA, D. S. DARROW[1], A. EJIRI[2], A. FUJISAWA, M. FUJIWARA, M. GOTO, K. IDA, H. IDEI, H. IGUCHI, N. INOUE, M. ISOBE, K. ITOH, S. KADO, K. KHLOPENKOV[3], T. KONDO[3], S. KUBO, A. LAZAROS[4], S. LEE, G. MATSUNAGA[5], T. MINAMI, S. MORITA, S. MURAKAMI, N. NAKAJIMA, N. NIKAI[5], S. NISHIMURA, I. NOMURA, S. OHDACHI, K. OHKUNI[5], M. OSAKABE, R. PAVLICHENKO[3], B. PETERSON, R. SAKAMOTO, H. SANUKI, M. SASAO, A. SHIMIZU[5], Y. SHIRAI[3], S. SUDO, S. TAKAGI[5], C. TAKAHASHI, S. TAKAYAMA[3], M. TAKECHI[5], K. TANAKA, K. TOI, K. YAMAZAKI, Y. YOSHIMURA, T. WATARI

National Institute for Fusion Science,
Toki 509-5292,
Japan

Abstract

The configuration parameter of the plasma position relative to the center of helical coil winding is very effective one to control the MHD stability and the trapped particle confinement in Heliotron/Torsatron systems. But these two characteristics are contradictory in this parameter to each other. Inward shifted configuration is favorable for the drift-orbit-optimization but it is predicted unstable with the Mercier criterion. Various physics problems, such as an electric field structure, plasma rotation, MHD phenomena, have been studied in CHS with a compromising intermediate position. With this standard configuration, CHS has supplied experimental results for understanding general toroidal confinement physics and low-aspect-ratio helical systems. In the recent experiments, it was found that the wide range of inward shifted configurations gives stable plasma discharges without any restriction to the special pressure profile. Such enhanced range of operation made it possible to study experimentally the drift-orbit-optimized configuration in the Heliotron/Torsatron systems. The effect of configuration improvement was studied with plasmas in a low collisionality regime.

1. INTRODUCTION

CHS (Compact Helical System) is a small low-aspect-ratio Heliotron/Torsatron device ($A_p \sim 5$) [1]. Since its construction at ten years ago, various plasma physics experiments have been conducted. The main objective was to confirm the advantage of low-aspect-ratio design of Heliotron/Torsatron system and to supply the experimental database for the next generation helical system LHD [2]. A large part of scientific achievement in helical system research that supported the decision of constructing LHD came from the Heliotron-E experiments. Since

---

1) Princeton Plasma Physics Laboratory, Princeton, N. J., U.S.A.
2) The Graduate School of Science, Tokyo Univ., Tokyo 113-0033, Japan
3) The Graduate Univ. for Advanced Studies, Toki 509-5292, Japan
4) National Technical University, Athens, Greece
5) Dep. of Energy Eng. Science, Nagoya Univ., Nagoya 464-8603, Japan

there was a large difference in the aspect ratio between two machines (A_p ~ 11 for H-E and A_p ~ 6.5 for LHD), the scientific experience of CHS experiment was very important to proceed to LHD. Dataset of global confinement of CHS have been incorporated into the world-wide stellarator scaling study [3] and it confirmed that confinement capability of CHS is on the general scaling line of global confinement for helical systems. A low-aspect-ratio design of Heliotron/Torsatron system generally gives the higher MHD stability limit. CHS achieved highest beta value of helical systems [4] and showed the possibility of realizing the stable discharge with a necessary beta for helical reactor designs.

A compactness of the device gave also benefits to the practical aspect of the experiments. It is possible to have a minimum requisite size of minor radius (a ~ 0.2 m) with a relatively small machine size (R = 1 m). This size of minor radius is necessary to clearly separate the core plasma confinement from the various physical processes in the plasma edge region. An advantage of small size device is great especially when a new topic of physical research is planned. The preparation of hardware can be done quickly and with a relatively small cost. Typical examples are new diagnostic tools which have been installed in CHS. They opened new area of physics research in helical systems : the HIBP (heavy ion beam probe) for the electric field study [5], the TVCXS (charge exchange spectroscopy with CCD camera) for the plasma rotation and electric field study [6] and the TESPEL (tracer-encapsulated solid pellet injection) for the precise transport study with the impurity injection [7]. The machine operation is flexible for a small size device. The H-mode was studied in the discharges with inductive current which was produced by swinging poloidal field [8]. The dynamic plasma position control for high beta plasma was also demonstrated [4].

The flexibility of magnetic field configuration control of CHS enables the optimization study of magnetic field structure. Although the range of configuration space is limited, the optimization for the drift orbits of deeply trapped particles is possible in the experiment. The essential problem for such optimization in Heliotron/Torsatron systems is the contradiction of drift orbit optimization and the MHD stability. In CHS, the stability of discharges, which is more stable than the limit from the Mercier criterion, gives much wider configuration space and enables the drift-orbit-optimization study. The effect of higher harmonic ripples in the vicinity of magnetic axis is clarified in the experiments in a low collisionality regime.

2. MAGNETIC CONFIGURATION OF CHS DEVICE

In Heliotron/Torsatron configuration, considerable amount of deeply trapped particles in the helical ripples do not escape directly from the confinement region. They drift around following the helical structure of magnetic field strength. But such drift orbits and the magnetic surfaces do not always coincide and the deviation of trapped particle orbits from the magnetic surfaces causes the ripple transport processes for low collisionality plasmas. This problem depends on the structure of helical windings. CHS has two helical windings ($\ell = 2$) with eight toroidal periods (m = 8). These helical coils produce the vacuum rotational transform $\iota = 0.3$ at the center and 1.0 at the boundary. A large pitch modulation of helical winding ($\alpha^* = 0.3$) is adopted for CHS device as shown by the winding law of helical coils given by Eq. (1).

$$\theta = N\,\phi + \alpha^* \sin(N\,\phi),\quad N = m/\ell, \tag{1}$$

where θ is the toroidal and ϕ is the poloidal angle, respectively. A pitch modulation gives two opposite effects depending on its sign. A negative sign enhances the helical ripples in the inboard side of torus which gives better coincidence of drift orbits to magnetic surfaces. But

such modification of helical winding reduces the size of the last closed magnetic surface (LCMS). Since the most important subject of CHS was to realize a low-aspect-ratio helical device, a positive number of α^* was selected. From this point of view, CHS has a negatively optimized magnetic field configuration for trapped particle orbits.

Even with a given helical coil structure, the characteristics of magnetic field configuration can be largely varied with a poloidal field control. CHS has three sets of poloidal coils which make it possible to control three free parameters in poloidal field (vertical field, quadrupole field, ...). Because the drift orbits of deeply trapped particles are determined by the structure of magnetic field strength, they are much less sensitive to the vertical field settings than the magnetic surfaces. Therefore, it is possible to coincide approximately the magnetic surfaces and the drift orbits by controlling magnetic surfaces with the poloidal field. In CHS, such configuration can be obtained by largely shifting the magnetic surfaces to the inboard side of torus.

Several magnetic surface characteristics which are important for the confinement study are shown in Fig. 1 as a function of the magnetic axis position R_{ax}[1]. The plasma volume is maximum at R_{ax} = 98 cm which is supposed to be the standard configuration from the viewpoint of making a fat plasma in a small device. The minimum aspect ratio 4.5 is obtained at the same position. The magnetic well is formed in the central region of a vacuum field when R_{ax} > 95 cm. The edge region is stabilized by the magnetic shear. The magnetic well is also increased by the Shafranov shift of magnetic axis for finite beta plasmas. The radius of magnetic well region is plotted in Fig. 1 for both vacuum field and the equilibrium with 1 % average beta. The profile of rotational transform varies depending on R_{ax} parameter. The magnetic shear parameter is largest at R_{ax} = 96 cm and decreases for both the outward shift and the inward shift of magnetic axis.

Most of magnetic axis positions in Fig. 1 are smaller than the major radius of helical coil winding (R = 1 m). It is because of the low aspect ratio characteristics of CHS and the positive pitch modulation of the helical coils. For the standard and inward shifted configuration (R_{ax} < 97 cm), the LCMS is determined by the inboard side of the vacuum vessel wall working as eight symmetric limiters. For the outward shifted configuration, the LCMS is given by the magnetic separatrix.

Drift orbits of deeply trapped particles are approximately illustrated using the Mod-B minimum plots which is a contour plots of minimum magnetic field strength along the field line within one helical period. A normalized radius of Mod-B minimum contour line enclosed by the LCMS is plotted also in Fig. 1. R_{ax} = 87.7 cm gives the best configuration for this point of view although sacrificing plasma volume and the magnetic well. The field ripple on the magnetic axis is also important for the neoclassical heat transport and the parallel viscosity of the plasma rotation. It comes from two effects of both helical excursion of magnetic axis (toroidal effect) and the variation of distance between the helical coils and the magnetic axis (helical effect). The dependence is shown in Fig. 1.

Large part of discharges in CHS have been produced with R_{ax} = 92.1, or 94.9 cm

---

[1] Rax is defined as the major radius of a magnetic axis at the vertically elongated toroidal cross section in the vacuum field. It is an operational parameter which reflects the setting of currents in helical and poloidal coils. It does not give real position of magnetic axis for a finite beta equilibrium.

since these configurations gave best performance for both NBI and ECH plasmas in CHS. Such range of magnetic axis position is a standard selection of Heliotron/Torsatron systems to compromise both the MHD stability and trapped particle orbits. This paper describes the experimental results to compare discharges in these standard configurations and more inward shifted configurations which gives the drift-orbit-optimization for Heliotron/Torsatron systems.

3. CONFINEMENT CHARACTERISTICS IN STANDARD CONFIGURATION

The database of CHS global confinement time which was incorporated in the international stellarator scaling study (ISS-95) [3] was taken from the discharges with standard configurations (R_{ax} = 92.1 or 94.9 cm). For this study, because the collisionality of most discharges were in the collisional or plateau regime, the characteristics of trapped particle orbits did not make large effect. More important aspects are anomalous transport and the engineering feasibility of efficient plasma heating. By contributing to the global confinement scaling, CHS assured the possibility of designing helical system with a low aspect ratio. It is important basis in planning a compact helical reactor. Two directions of helical system research for both a high aspect ratio (Ap ~ 10) and a low aspect ratio (Ap ~ 3 - 4) became possible.

The global confinement time of collisional plasma is better with the standard configuration than the outward shifted one (R_{ax} > 95 cm) even if the plasma volume is smaller than R_{ax} = 98 cm [9]. This result is opposite to the common understanding of global confinement in the relation with the MHD stability. In this respect, the magnetic well does not assist better confinement in CHS. On the other hand the global confinement stays on the similar level for the inward shifted configuration (R_{ax} < 92 cm) even though the ideal MHD stability becomes worse. It should be noted that there remains some ambiguity in evaluating the heating efficiency because the behavior of high energy particles are difficult to fully understand both for ECH and NBI heated plasmas. The confinement characteristics of less collisional plasmas will be discussed in Section 6.

A typical electron temperature and density profiles of ECH plasma are shown in Fig. 2. The output power of 106 GHz gyrotron was 300 kW and the magnetic field was 1.9 T on the magnetic axis in the standard configuration R_{ax} = 92.1 cm. The double folded structure is noticed in the temperature profile. Such structure is general for ECH plasmas in CHS and a much clearer example is obtained for a low density plasma ($n_e \sim 2 - 3 \times 10^{12}$ cm^{-3}) with the electric potential profile measurement by HIBP [10]. The electric potential showed the similar double folded profile. The collisionality of helical ripple trapped particles is less than unity at a half radius in Fig. 2, and the experimentally obtained electron thermal conductivity is close to the neoclassical value ($\chi_e \sim 3$ m^2 sec^{-1}).

The highest ion temperature was obtained in the high Ti mode experiments in CHS [11] using NBI heating. The profile of ion temperature measured by TVCXS diagnostics is shown in Fig. 3 together with the electron temperature and density profiles. The magnetic field was 1.9 T and the configuration with R_{ax} = 92.1 cm was selected. Single co-injection beam was used with a careful tuning for the better beam focusing. Strong wall conditioning with the titanium gettering was necessary to suppress the wall recycling which resulted in the peaked density profile mostly fuelled with the injected beam.

CHS has two neutral beam injectors (NBI #1 and #2), the maximum energy of which are 40 keV and 36 keV respectively. Two beams are installed so as to make a balanced tan-

gential injection. One system (NBI #1) is movable to allow various injection angle to the magnetic field for the purpose of high energy particle confinement study. The ratio of the ion Larmor radius to the plasma minor radius is 1/6 to 1/7 for 1 T operation (1/30 for LHD with E_0 = 180 keV and B_t = 3 T). In the case of tangential injection the toroidal shift of the passing orbit of the beam ions from the magnetic surface becomes 1/2 to 1/3 times minor radius. Combined with large Larmor radius size, the real trajectories of beam ions show very complicated structure especially for the passing boundary particles. As an example, an orbit of a co-injected beam particle with a pitch angel of 60 degree at r/a = 0.2 is shown in Fig. 4. It makes an excursion out of the LCMS on the outboard side of torus, and comes back into inside of the LCMS.

Those particles play an important role not only in the plasma wall interaction, but also in the charge exchange loss of the beam particles. On CHS, an escaping particle probe which resolves the gyro-radius and pitch angle was installed and these particles were studied [12, 13]. Generally, the signal strength of the escaping passing boundary particles shows a similar time evolution to that of plasma pressure.

The pressure of high energy beam ions is large for most of NBI discharges. For low density discharges, total energy of beam components is comparable to the thermal energy of plasmas. Various MHD phenomena are observed which have the close relation to the beam components. Beam driven TAE mode was found in CHS for the first time in helical devices [14], which has the close relation to the GAE mode found in Wendelstein 7-AS [15]. Another topic in this field is fishbone like MHD oscillations [14, 16]. This oscillation is observed only for the co-injection of the beam. One possible reason is the difference of the rotational transform profile for the co-injection and the counter-injection. The observed beam driven current was about 10 kA which may change the rotational transform by about 5 %.

Toroidal plasma rotation driven by the tangential NBI was studied experimentally and gave the understanding of neoclassical parallel viscosity due to the magnetic field ripples (TTMP effect). The rotation depends largely on the configuration because of the different ripple structures. Figure 5 shows the toroidal plasma rotation speed driven by the co- and counter-beam as a function of R_{ax} [17]. The maximum speed was observed for the configuration with R_{ax} = 89.9 cm where the field ripple is minimum as shown in Fig. 1 in Section 1. A more complete calculation of neoclassical parallel viscosity was made based on the magnetic surface averaging of the field gradient γ (= < dB/ds >) at r/a = 0.2 which is plotted in Fig. 5. The dependence of measured rotation speed on R_{ax} is consistent with this calculated viscosity if the perpendicular viscosity of 0.2 m^2/s is added to slightly modify the profile of rotation. The standard configuration of CHS allows a large toroidal rotation speed which might be some help for getting better global confinement.

It was found in the perpendicular beam injection experiments and ICRF heating experiments that the confinement of perpendicular high energy ions is bad in the standard configuration of CHS. In the NBI experiments, NBI #1 which was set in the perpendicular injection could not heat the plasma at all [18]. On the other hand, the ICRF experiments were successful in CHS only if the experimental scenario of electron heating was adopted [19]. These results are consistent to the theoretical analysis of trapped particle orbits for the standard configuration.

In order to solve these problems, the experiments were planned to extend the operational range of magnetic axis position R_{ax}. An optimized configuration for the deeply trapped

particles is obtained with R_{ax} = 87.7 cm. A mod-B minimum contour plot for this configuration is shown in Fig. 6 with a plot for the R_{ax} = 92.1 cm as a reference. The plots are made for the magnetic coordinates. To achieve a good coincidence of drift orbits with the magnetic surfaces which is shown in Fig. 6a, a control of quadrupole component of poloidal field is necessary. The toroidally averaged flux surfaces of Fig. 6a are almost circular while the standard configuration shown in Fig. 6b has a small vertical elongation of the averaged magnetic surfaces.

The magnetic field ripple structure for the drift orbit optimized configuration is shown in Fig. 6c for three different minor radii. The minimum values of field strength at all bottoms of ripples are almost constant. Such feature was discussed many years ago in terms of the σ-optimization of the helical magnetic field [20]. More advanced optimization of helical field requests the alignment of the field strength of magnetic field ripples both at their maxima and minima, which is called quasi-omnigenous. It is impossible to make a quasi-omnigenous optimization in CHS based on its existing helical coils. Since the plasma parameters we can obtain in most experiments are in the barely collisionless regime, a halfway optimization shown in Fig. 6 should be effective for improving the confinement.

4. ELECTRIC FIELD IN THE STANDARD CONFIGURATION

The effect of electric field on the confinement has been discussed in helical systems from the very early phase of its research. It was in the framework of neoclassical transport which is different from the discussion of the effect of electric field shear on the anomalous transport. In helical devices, because the anomalous effect is still large for the transport, both aspects of electric field are important. Large efforts have been made in CHS for the development of diagnostic tools of electric field measurements. The TVCXS measured impurity flow profiles (mostly with carbon impurity) both in poloidal and toroidal directions and gave information of electric field profiles [21]. This diagnostics worked well for the middle and high density plasmas heated by NBI. The HIBP measured full profiles of electric potential for both ECH and NBI plasmas with a relatively low density [22]. Figure 7 shows the electric field profiles of NBI plasmas measured by TVCXS for three different densities. The magnetic field was about 0.9 T with standard configurations. Stronger electric field was observed for the higher density plasmas. The profile shape and the strength of the electric field is consistent to the neoclassical theory prediction.

The potential profiles for ECH and NBI plasmas measured by HIBP are shown in Fig. 8 for the magnetic field 0.88 T with a standard configuration R_{ax} = 92.1 cm. The Radial electric field is positive in the central region of ECH plasmas. The potential profile with stronger ECH shows a double folded structure which corresponds to the similar electron temperature profile mentioned in Section 3. The effect of electric field on the neoclassical heat transport has not been clearly identified in the comparison of heat transport coefficient obtained from the experiment with the neoclassical model. The electric field shear at the boundary region of higher density ECH plasma is 50 V/cm^2 which is expected to contribute to the reduction of anomalous transport by about 10 % [10].

HIBP can measure the potential profile of NBI only for the density lower than 2×10^{13} cm^{-3}. It is because the radiation from the plasma disturbs the measurement of secondary ionized beam. On the other hand TVCXS has a difficulty of measuring the electric field for low density NBI plasmas because the electric field is very small for these plasmas. Simultaneous measurements of both diagnostics were made for the intermediate density NBI plasma successfully.

The solid line in Fig. 7 shows the electric field profile calculated from the potential profile measurement by HIBP for the NBI plasma shown in Fig. 8. The discrete points are plotted from the measurement by TVCXS. These two diagnostics show good agreement with each other for this range of density.

Another effect of electric field on the confinement in helical systems is the resonant loss of high energy trapped particles. Because the radial electric field of NBI plasmas is negative, the $E \times B$ motion and the curvature drift motion are cancelled out for a particular energy which causes the direct loss of trapped particles. The energy spectrum of fast neutral particles which have almost perpendicular pitch angles is shown in Fig. 9a for the high magnetic field experiment (B_t = 1.76 T). It has a dip in the range from 2 to 4 keV. Tail components in the higher energy range come from tangentially injected high energy beam ions. This dip appeared only when the strong ion heating occurred. Exponential fitting (shown by the line in the figure) of the perpendicular spectrum in the energy range of $0.45 < E_0 < 1.2$ keV (below the dip energy) gave almost the same ion temperature as the TVCXS gave. Energy spectrum for the measuring angle shifted by 16 degrees (denoted by 'oblique') is also shown in the figure for the comparison. The dip of the spectrum disappeared in this case. Because the spectrum with an intermediate measuring angle showed about 70 % dip compared with the perpendicular case, the width of the resonant loss cone is of the order of 10 degree. The spectrum dip position corresponds to the calculated particle energy for the resonant loss process.

Plasma potential control for NBI plasmas with the application of ECH was demonstrated in CHS in 1992 [23]. The electric field changed from negative to positive during the application of ECH on NBI plasmas. Similar control was made for this plasma by applying 200 kW 53 GHz ECH in the low field experiment (B_t = 0.88 T). Time variation of the local slope of the fast neutral particle energy spectrum (explained by an equivalent temperature in the energy range from 1 to 2 keV) is shown in Fig. 9b for the perpendicular pitch angle measurement. During ECH, this slope became smaller (higher equivalent temperature) which is the indication of decrease of the dip in the spectrum. The reduction of carbon impurity was also observed during ECH pulse. However the ion temperature did not show any significant increase during ECH which indicate that the resonant loss of ions in CHS is still negligible compared with the total energy loss mechanisms of ions.

The electric field has been measured for various discharges in CHS. The profiles are consistent to the neoclassical particle flow modelling for most cases. However the comprehensive evidence of confinement improvement with the electric field has not been obtained so far in CHS because the separation of anomalous loss from the neoclassical transport is difficult for most discharges. Nevertheless some observations were made which showed the coincidence of electric field structure and the temperature profile. One example is high power ECH plasmas which showed double folded structure both in the potential and temperature profiles. In this case, because the contribution of central part of a plasma to the total energy is small, the improvement of global confinement is not noticeable. Another example is in the high Ti mode experiments which showed the coincidence of transition from L mode to high Ti mode with a significant change of electric field profile [11].

5. MHD STABILITY OF OPTIMIZED CONFIGURATION

In the discussions of the experiment operation scenario of Heliotron/Torsatron devices,

largely inward shifted configurations are usually excluded because they are (supposed to be) not MHD stable. The ideal interchange stability of Heliotron/Torsatron systems is given by the combination of magnetic well and magnetic shear stabilizing effects. It is general tendency for all Heliotron/Torsatron devices that the stability is lost when the magnetic surfaces are shifted inward because the magnetic well disappears and the magnetic shear is decreased. It has been discussed that there is no good compatibility of the drift-orbit-optimization and the MHD stability for Heliotron/Torsatron systems.

NBI discharges in CHS appeared to be more stable than the prediction of the ideal interchange stability theory. Discharges in the configurations which have large Mercier unstable area in the central region were obtained without any instability. Figure 10 shows beta values and the plasma boundary positions of selected discharges from the series of experiments of drift-orbit-optimization. The plasma boundary position R_{00} is defined as an averaged major radius of the last closed magnetic surface[2]. The R_{ax} parameters for the vacuum cases are shown below the R_{00} values for the comparison between them. Two thick lines in the figure indicate the boundary of the ideal interchange stability from the Mercier criterion. The right side of the solid line (outward shifted configuration) is the region where the equilibrium is Mercier stable for whole plasma region. The equilibrium in the left side has at least one unstable magnetic surface for the interchange mode. Since the low mode instabilities are most dangerous ones, there is a region of low growth rate of such mode which is practically stable for the laboratory plasmas even with the Mercier unstable condition. A thick dotted line gives such a low mode stability boundary. The drift-orbit-optimization shown in Fig. 6 is realized at the plasma boundary position $R_{00} = 90$ cm. The square and circle points are the data points with NBI and ECH heating respectively. They are all stable discharges though the Mercier stability analysis predicts unstable.

Three triangles in Fig. 10 are taken from the high beta experiments in CHS [4]. An example of the plasma movement is shown by an arrow for the discharge which became Mercier stable as the plasma beta increased (second stability for the interchange mode). The Mercier stability generally becomes better when the plasma beta increases because of the outward shift of the plasma position and the creation of magnetic well due to the Shafranov shift. Fig 10 shows that discharges in the inward shifted configuration of CHS were already stable even before getting the second Mercier stability. There is a first stability region for very low beta values given by the magnetic shear stabilization effect. But such region is limited for very low beta and is below beta values of ECH discharges shown in the figure.

The ballooning stability analysis was made for the high beta discharges in Fig. 10 [24]. The calculated stability boundary was close to 2 % beta for strongly localized structure in toroidal direction. However, since the toroidal Fourier modes for such structure are very high, it is predicted that these modes would not be excited in the real laboratory plasmas. The magnetic fluctuations were measured for various beta values in the experiments. The fluctuation level increased as the beta increased but it was saturated in the amplitude when the beta became close to 2 % [25, 16]. Because the fluctuation measurement was made with a poloidal array of magnetic probes which was installed at the toroidal cross section where the ballooning mode is

[2] Plasma position is denoted here by the position of LCMS from the finite beta equilibrium instead of Rax because this parameter is closely related to the MHD stability.

localized, the saturation of magnetic fluctuations at 2 % beta implies the ballooning mode did not limit the beta. The consideration of power balance including the heating efficiency of NBI could explain the obtained beta value of 2 % [26].

The MHD stability analysis largely depends on the pressure profile of discharge. Because the stabilization due to the magnetic shear works in the boundary region even for the inward shifted configuration, an artificial pressure profile which has a very flat shape in the central region and has a pressure gradient localized only in the boundary region could be Mercier stable. Profiles of temperature and density were measured carefully for all discharges shown in Fig. 10. Two typical examples are shown in Fig. 11 for the standard configuration (R_{ax} = 92.1 cm) and for the drift-orbit-optimized configuration (R_{ax} = 87.7 cm). No essential difference is found between two configurations.

In the equilibrium calculation for the stability analysis, the beam pressure profile calculated with a beam deposition code is added to those kinetic pressure. Since the beam pressure in CHS gives a large part in total pressure, there remains an ambiguity in pressure profiles from this part. Total pressure profiles were in the range of normal profiles observed in CHS experiments which can be described by the formula : $p(r) \propto (1 - r^2)^{\alpha}$ with $1.5 < \alpha < 2.5$. This difference of profile shape does not make any essential effect to the stability conclusion except the difference in the ratio of average beta and the central beta values. Difficulty of modelling also comes from the large toroidal shift of passing beam trajectories which causes the nonuniformity of beam pressure on a magnetic surface. Though the contribution of the anisotropic beam pressure to the MHD stability is also important, it usually excites instability (e.g., MHD modes described in Section 3) and it is difficult to find the stabilizing effect given by the beam component.

The Mercier stability map for the R_{ax} = 88.8 cm is shown in Fig. 12 calculated with the pressure profile : $p(r) \propto (1 - r^2)^2$. The contour lines of a Mercier criterion D_I [27] is plotted for $D_I = 0$ and $D_I = 0.2$. Magnetic surfaces inside $D_I = 0$ contour line for a given beta are unstable for a Mercier criterion. $D_I = 0.2$ contour line gives the low mode stability boundary [28] which corresponds to the dotted line in Fig. 10. Thin dotted lines are also drawn in Fig. 12 to show the positions of particular radii : the boundary of magnetic well and the positions of low number rational surfaces of 1/2 and 2/3. A magnetic surface with $\iota = 1$ disappears for this inward shifted configuration. Finite beta equilibrium was calculated using the free boundary VMEC code [29] with a vacuum field of R_{ax} = 88.8 cm configuration. Due to the outward shift of the boundary and the Shafranov shift, the equilibrium finally gets into the second stability region when the beta reaches 2 %. But the experimental condition shown in Fig. 10 is in the unstable region from the Mercier criterion.

Figure 13 shows magnetic fluctuations measured for NBI discharges shown in Fig. 10 as a function of plasma beta. There are different types of magnetic fluctuations in CHS [14] which were excited either by pressure gradient or the high energy beam ions. But generally the total fluctuation level is larger for the inward shifted discharges than for the outward shifted ones for $R_{00} > 92$ cm [16]. However for those discharges shown in Fig. 13 ($R_{00} < 92$ cm) they did not increase even though the Mercier stability condition became worse as the plasma position is moved inward.

Beta values achieved for these discharges are lower than the one obtained for the R_{ax} = 92.1 cm configuration. It is mostly because the experiment time for the operation of these

optimized configuration was not sufficient to achieve as good machine condition as the high beta experiment campaign with the standard configuration. A reduced plasma volume is also a disadvantageous point in the heating efficiency and the wall effects for the high density operation.

Small disruptive drop of density and energy were observed in discharges with the inward shifted configuration R_{ax} = 88.8 cm. But such phenomena could not be observed frequently even when the plasma gets close to the highest obtainable beta value for a particular configuration. There might be hidden parameters for such instability which have not been clearly understood.

6. CONFINEMENT OF OPTIMIZED CONFIGURATION

The effect of confinement improvement by the drift-orbit-optimization was studied with ECH plasmas with plasma parameters in the low collisionality. Beta values of these plasmas are order of 0.1 % and the magnetic field configuration is almost the same as the vacuum configuration. The radial structure of major ripple components are shown in Fig. 14 for the standard configuration (R_{ax} = 92.1 cm) and the optimized one (R_{ax} = 87.7 cm) in addition to the mod-B minimum contour plots already shown in Fig. 5 in Section 3. A mirror ripple component (poloidal mode is zero) appears in the R_{ax} = 87.7 cm although it is very small for R_{ax} = 92.1 cm. Because, in central region of the standard configuration, all ripples are considerably small compared to the toroidicity, the transport in the central region is supposed to be dominated by the one for the axisymmetric torus. The transport due to helical ripples is important in the region of r/a = 1/3 ~ 2/3. For the region from a half radius to the boundary, the anomalous transport becomes more and more dominating.

Series of ECH discharges were made for several R_{ax} parameters between the optimized configuration and the standard one. 200 kW heating power of 53 GHz frequency was used with a good microwave beam focussing at the magnetic axis (half width of gaussian profile for the electric field is 1.5 cm in the poloidal direction). The magnetic field strength on the axis was 0.95 T. The single-path absorption is estimated to be about 70 % for the typical plasma parameters in the experiments. The plasma density was set at $5 - 6 \times 10^{12} cm^{-3}$ to ensure the collisionless condition.

Figure 15 shows the plasma diamagnetic energy normalized by the plasma volume and the central electron temperature as a function of the position of magnetic axis R_{ax}. The normalized plasma energy increased as the R_{ax} is shifted inward which shows the confinement improvement. But it started to drop before getting to the final optimized configuration R_{ax} = 87.7 cm. On the other hand, the increase of the central electron temperature was observed only for R_{ax} = 91.1 cm and it decreased for the further inward shift.

Results of the transport analysis for R_{ax} = 92.1 cm is shown in Fig. 16. Figure 16a shows the profiles of collisionalities of ν_e^* and ν_e^{**}. ν_e^* is the collisionality for the toroidal banana orbit which is the ratio of the electron ion collision frequency ν_{ei} to ν_b, where $\nu_b = \varepsilon_t^{3/2} \iota/R\,(T_e/m_e)^{1/2}$. ν_e^{**} is the collisionality for the helical banana orbit where $\nu_e^{**} = \nu_{ei}/\nu_{eq}'$, $\nu_{eq}' = (\varepsilon_h/\varepsilon_t)^{3/4}\nu_b$. Fig 16b shows the calculated neoclassical heat transport coefficients together with the one deduced from the experimental observation of electron temperature profile. Three calculated profiles are shown in Fig. 16b for the transport coefficient which comes from the axisymmetric toroidicity, helical ripples and the sum of these. Since the calculation is based on the single helicity model, the effect of configuration optimization cannot be included.

From this calculation, it is expected that the neoclassical transport in the central region of R_{ax} = 92.1 cm configuration is dominated by the tokamak-like banana particle motions. But in the region near the half radius, transport caused by the helical ripples becomes more important. The increase of the global confinement for the inward shifted configuration comes from the improvement of transport near the half radius because the integration of this area is much larger than the contribution from the central region. The configuration optimization gave large effect to the transport in this region by suppressing the ripple diffusion of trapped particles caused by the drift motion. On the other hand, in the central region, the helical ripple diffusion is not dominating diffusion process for R_{ax} = 92.1 cm configuration. When the magnetic axis is shifted inward, ripple on the axis is increased as shown in Fig. 1 in Section 2. It is expected that the additional transport appeared due to the increased ripples near the magnetic axis. This might be the reason why the central electron temperature decreased for the inward shifted configuration.

Since the optimized configuration R_{ax} = 87.7 cm is strongly shifted to the helical coil on the inboard side of torus, a stochasticity of magnetic surface appears at the boundary with t = 0.8. It depends also on the quadrupole component. This effect is one of possible causes for the degradation of the global confinement for $R_{ax} < 89$ cm.

The effect of electric field in the neoclassical transport could be another key for understanding the confinement improvement (and the degradation) with the drift-orbit-optimized configuration. The measurement of electric potential for the optimized configuration is planned. The possibility of controlling the mirror ripples on the magnetic axis with additional perturbation coils is also under consideration.

7. CONCLUSION

Compact Helical System (CHS) experiment has extended the configuration range of helical confinement system to the low-aspect-ratio field. It is not only a necessary scientific support for continuing new LHD project in NIFS, but also a very important achievement for the future direction of helical confinement research on the way to the commercial reactor. The compactness is always the most important key issue.

CHS has developed new advanced diagnostics and fully utilized them to solve fundamental physics problems related to both the general toroidal confinement study and the confinement physics in helical systems. The structures of electric field and the plasma rotation were investigated in details and quantitatively. Transient phenomena of potential structure was also revealed. The transport is investigated with an active diagnostic tool of a pellet injection. Various kinetic MHD modes were studied which characterize plasmas confined in helical systems.

The improved confinement modes are found for both electron and ion confinement. The internal transport barrier was found for electron temperature profile which is related to the similar potential profile. The high Ti mode was found for NBI discharges which gave 1 keV ion temperature.

Wide range of configuration was studied for MHD stability and the confinement improvement. It was found that discharges in Mercier unstable configurations were experimentally stable in CHS. The methods of optimization for Heliotron/Torsatron system were investigated. The drift-orbit-optimization was tested with low collisionality plasmas and the effect of reduction of helical ripple transport was confirmed. The direction to a more advanced optimization is a future problem.

REFERENCES

[1] MATSUOKA, K., et al., Proc. 12th International Conference on Plasma Physics and Controlled Nuclear Fusion Research, Nice, 1988, Vol. 2, IAEA, Vienna (1989) 411-417.

[2] IIYOSH, A., et al., Fusion Technol. **17** (1990) 169-187.

[3] STROTH, U., et al., Nucl. Fusion **36** (1996) 1063-1077.

[4] OKAMURA, S., et al., Nucl. Fusion **35** (1995) 283-296

[5] FUJISAWA, A., et al., Rev. Sci. Instrum. **63** (1992) 3694-3700.

[6] IDA, K., HIDEKUMA, S., Rev. Sci. Instrum. **60** (1989) 876.

[7] SUDO, S., et al., this conference.

[8] TOI, K., et al., Proc. 14th International Conference on Plasma Physics and Controlled Nuclear Fusion Research, Wurzburg, 1992, Vol. 2, IAEA, Vienna (1993) 461.

[9] KANEKO, O., et al., Proc. 13th International Conference on Plasma Physics and Controlled Nuclear Fusion Research, Washington, 1990, Vol. 2, IAEA, Vienna (1991) 474.

[10] FUJISAWA, A., et al., Fusion Energy 1996 (Proc. 16th International Conference on Fusion Energy), Vienna, Vol. 2, (1997) 41-54.

[11] IDA, K., et al., this conference

[12] DARROW, D. S., et al., J. Plasma Fusion Res. SERIES, Vol. 1 (1998) 362-365.

[13] ISOBE, M., et at., to be published in Rev. Sci. Instrum. **70** (1999).

[14] TOI, K., et al., this conference

[15] WELLER, A., et al., Phys. Rev. Lett. **72** (1994) 1220.

[16] SAKAKIBARA, S., et al., J. Phys. Soc. Japan **63** (1994) 4406-4421.

[17] IDA, K., NAKAJIMA, N., Phys. Plasmas **4** (1997) 310-314.

[18] OKAMURA, S., et al., Proc. 14th International Conference on Plasma Physics and Controlled Nuclear Fusion Research, Würzburg, 1992, Vol. 2, IAEA, Vienna (1993) 507-514.

[19] MASUDA, S., et al., Nucl. Fusion **37** (1997) 53.

[20] Mynik, H. E., et al., Phys. Rev. Lett. **48** (1982) 322.

[21] IDA, K., et al., Phys. Fluids B **3** (1991) 515-518.

[22] FUJISAWA, A., et al., Phys. Plasmas 4 (1997) 1357-1361.

[23] IDEI, H., et al., Phys. Rev. Lett. **71** (1993) 2220-2223.

[24] NAKAJIMA, N., Phys. Plasmas **3** (1996) 4545-4555, 4556-4567.

[25] OKAMURA, S., et al., Proc. 15th International Conference on Plasma Physics and Controlled Nuclear Fusion Research, Seville, 1994, Vol. 1, IAEA, Vienna (1995) 381-388.

[26] MURAKAMI, S., et al., Nucl. Fusion 36 (1996) 359-365.

[27] GLASSER, A. H., GREENE, J. M., JOHNSON, J. L., Phys. Fluids **19** (1976) 567-574.

[28] ICHIGUCHI, K., et al., Nucl. Fusion **33** (1993) 481.

[29] HIRSHMAN, S. P., et al., Comput. Phys. Commun. **43** (1986) 143.

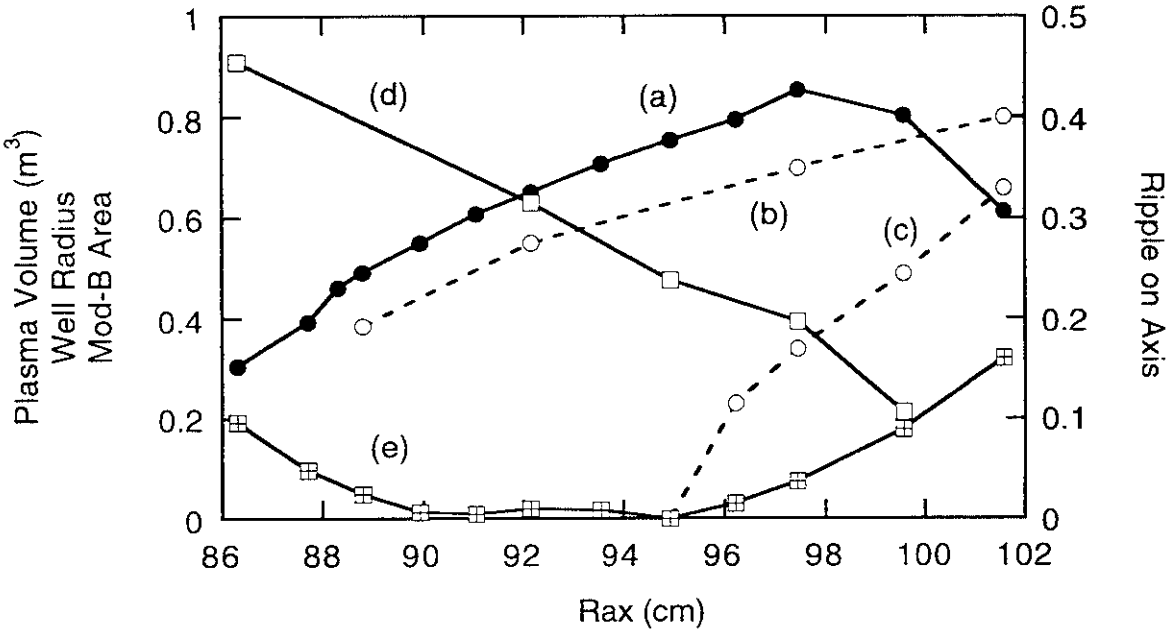

Fig. 1 Plasma volume (a), normalized radius of magnetic well region for 1 % beta (b) and for 0 % beta (c), relative area of closed Mod-B minimum contour (d), field ripple on magnetic axis (e), as a function of magnetic axis position R_{ax}.

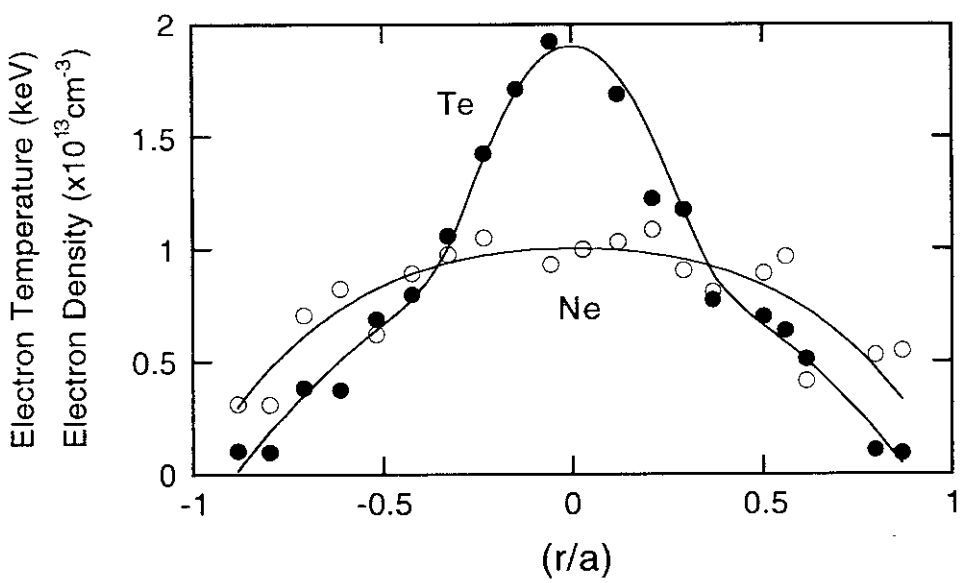

Fig. 2 Electron temperature and density profile for 106 GHz ECH heating. R_{ax} = 92.1 cm, B_t = 1.9 T.

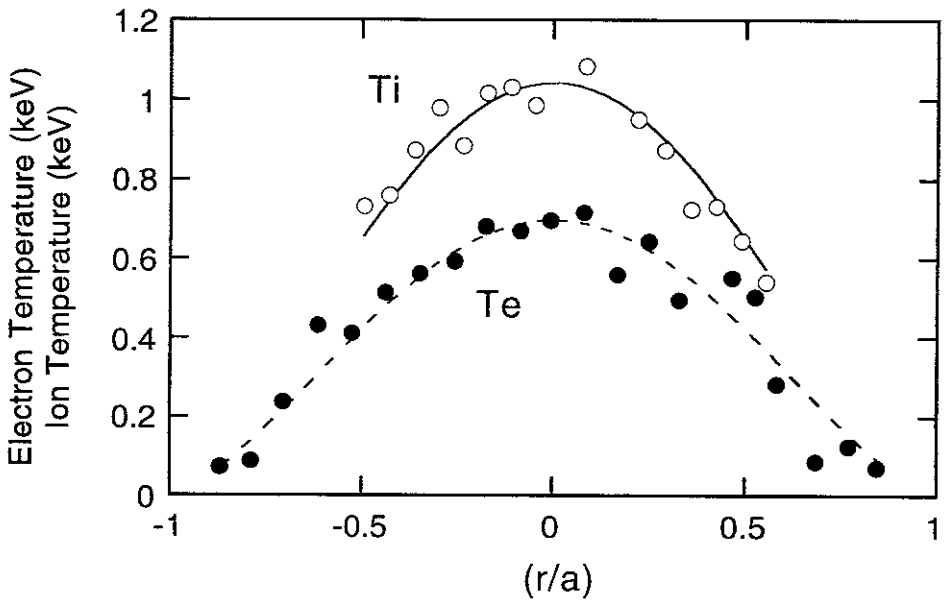

Fig. 3a Ion temperature and electron temperature profiles in high Ti mode experiment

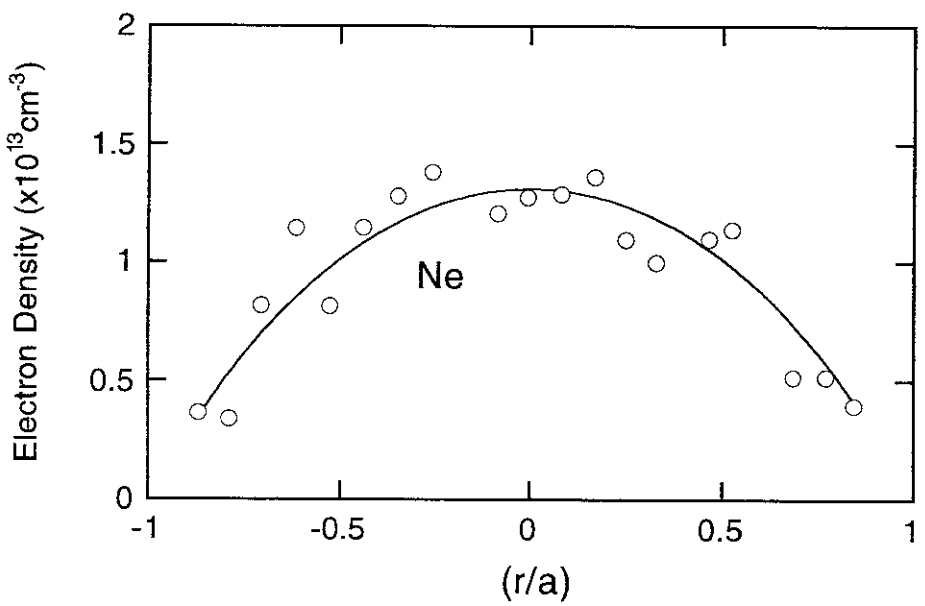

Fig. 3b Electron density profile in high Ti mode experiment

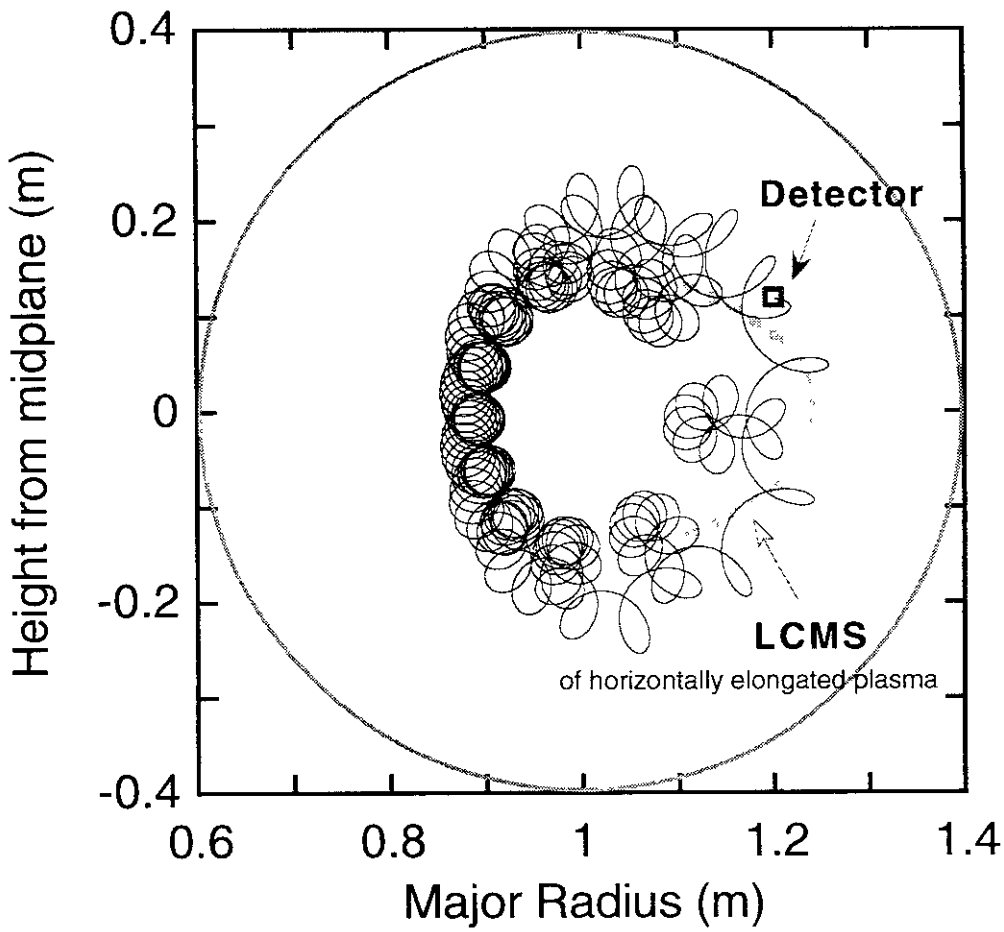

Fig. 4 Toroidal projection of full orbit trajectory for 38 keV proton with 48 degree pitch angle at detector position. The last closed magnetic surface is shown for the toroidal cross section where the escaping particle probe is installed. Magnetic field configuration is Rax = 94.9 cm and the magnetic field strength is Bt = 0.9 T.

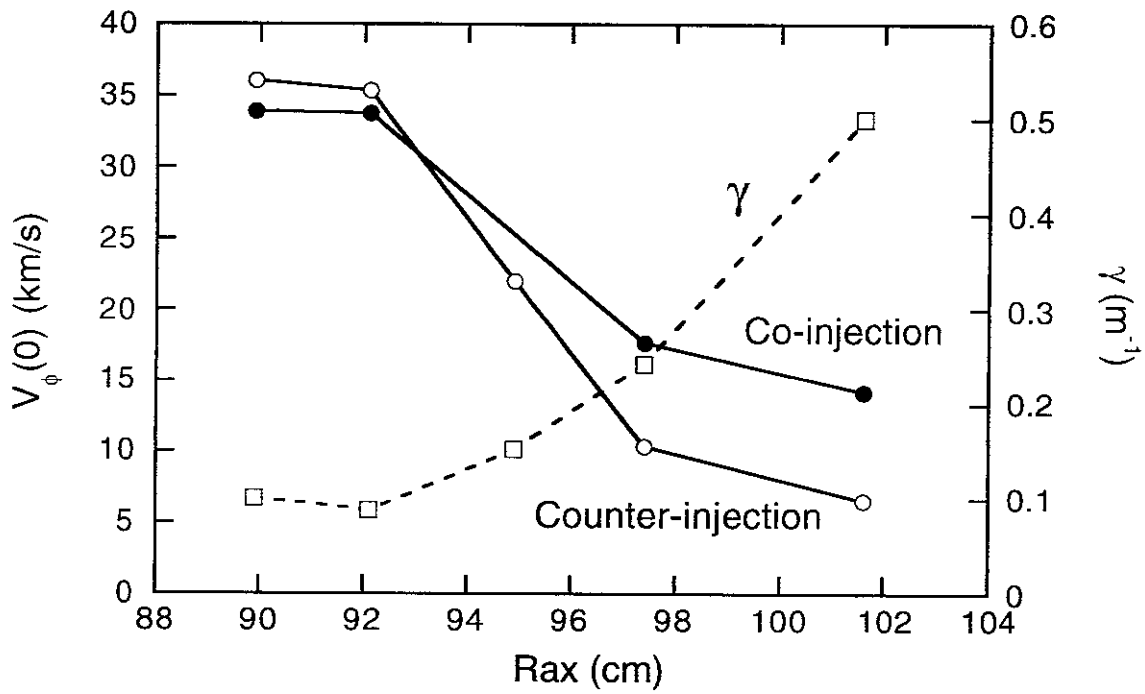

Fig. 5 Dependence of toroidal rotation velocity of plasma on magnetic axis position. Both co-injection NBI heating and counter-injection case are plotted. Averaged magnetic field gradient γ is also plotted for r/a = 0.2 magnetic surface.

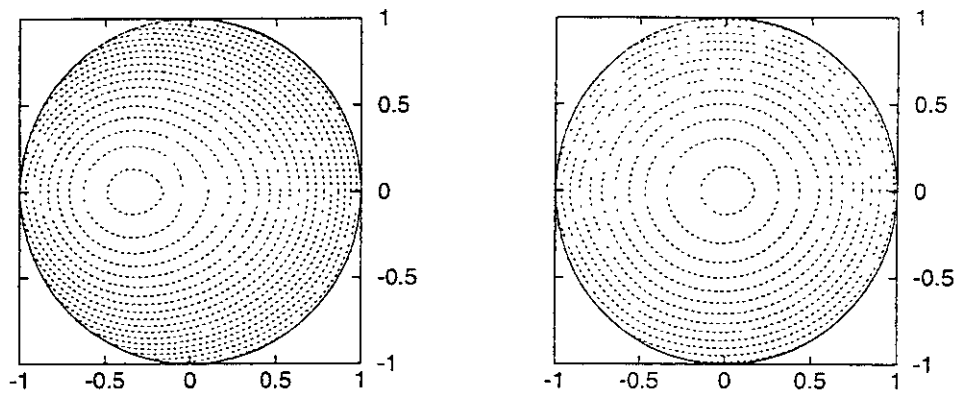

Fig. 6a Mod-B minimum plots for standard configuration R_{ax} = 92.1 cm and drift-orbit-optimized configuration R_{ax} = 87.7 cm.

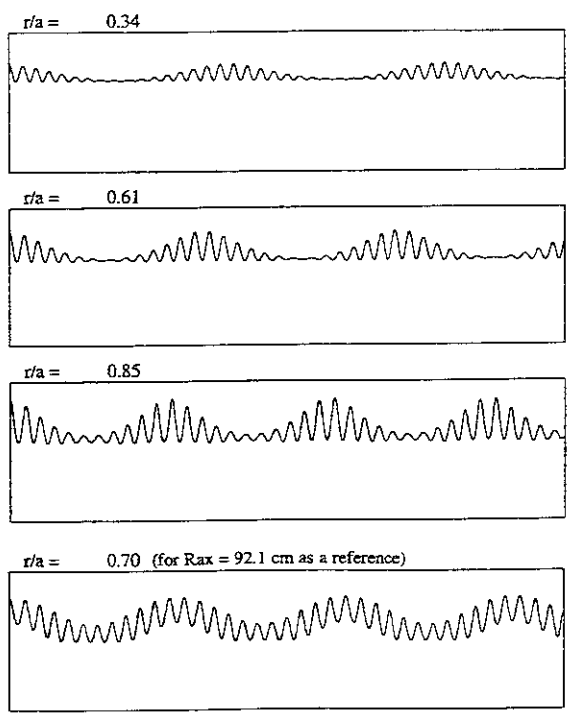

Fig. 6b Magnetic field ripple structure at three different minor radii for drift-orbit-optimized configuration R_{ax} = 87.7 cm. The ripple structure for standard cofiguration is also plotted for comparison.

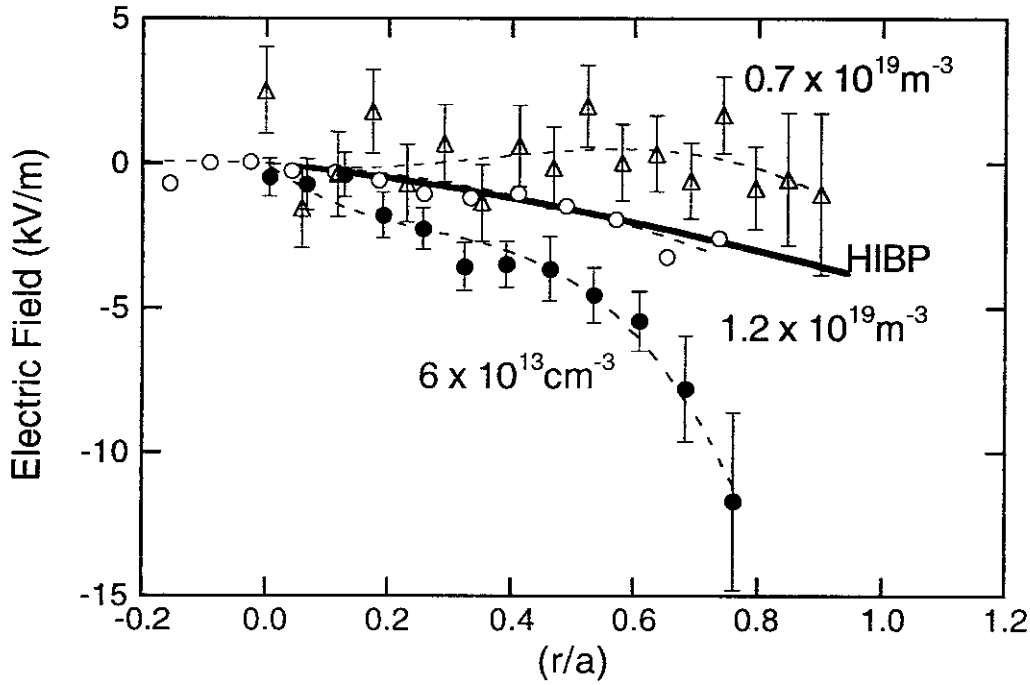

Fig. 7 Electric field measurements by TVCXS diagnostics for NBI plasmas with three different densities. Simultaneous measurement of electric field by HIBP is plotted with solid line for middle density case.

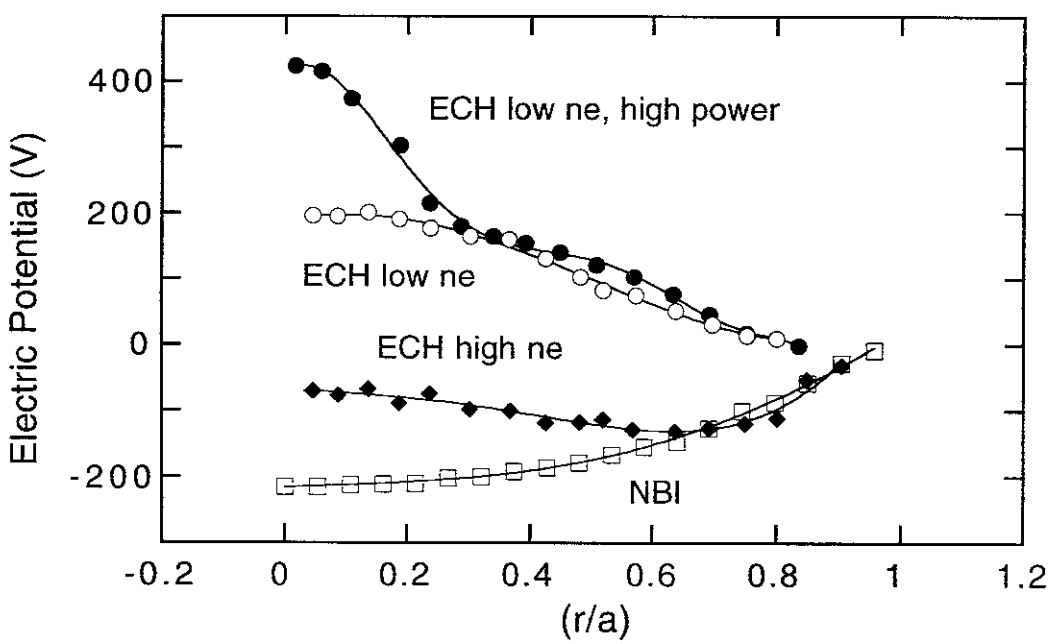

Fig. 8 Electric potential measurements by HIBP diagnostics. Electron densities for low n_e ECH was 3×10^{12} cm^{-3}, for high n_e ECH and NBI discharge, 8×10^{12} cm^{-3}. Input power for high power ECH was 300 kW while others were 100 kW.

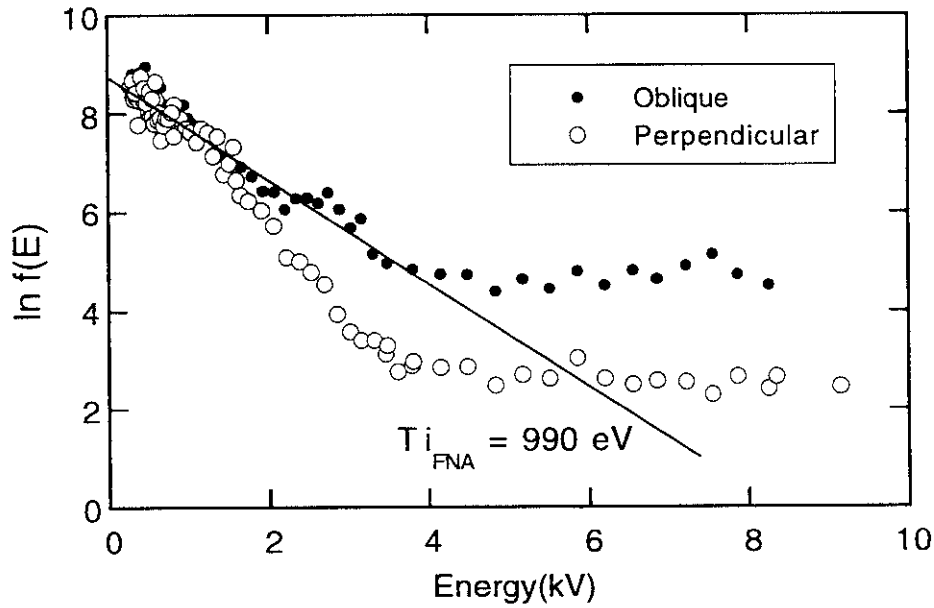

Fig. 9a Spectrum of fast neutral particles obtained by FNA diagnostic. Open circles are from the measurement with perpendicular observation antle to the magnetic field. Small closed circles are with 16 degrees shifted angle. Straight line is the result of spectrum fitting in the energy range : $0.45 < E_0 < 1.2$ keV for getting ion temperature. Magnetic field configuration was $R_{ax} = 92.1$ cm and the field strength was $B_t = 1.76$ T.

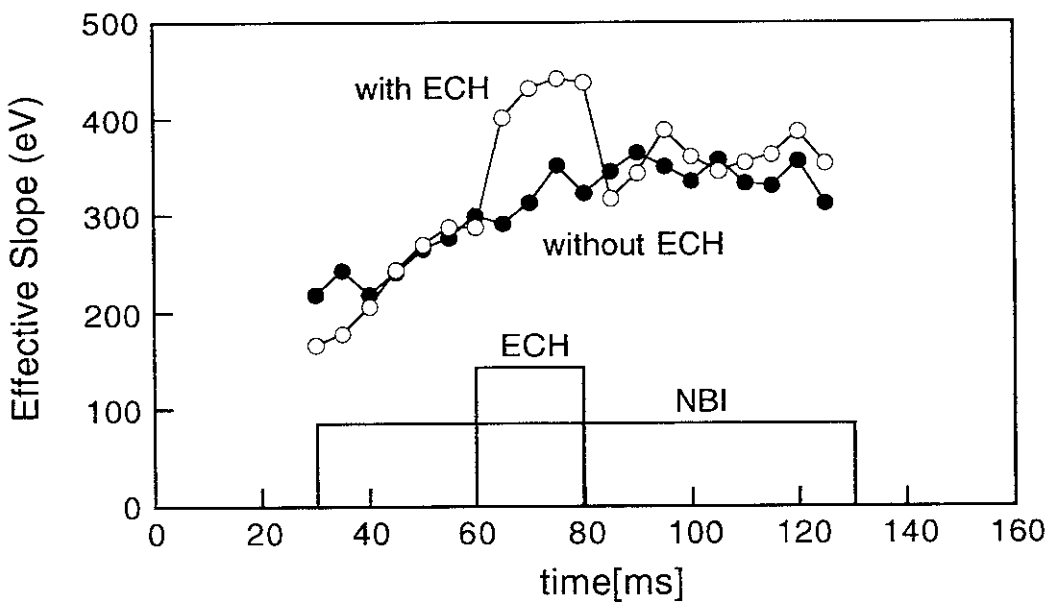

Fig. 9b Time variation of energy spectrum slope in the range of $1 < E_0 < 2$ keV for NBI discharges with and without ECH. The dip of energy spectrum was decreased by application of ECH. The ion temperature measured by TVCXS diagnostic was 600 eV at 70 msec. Magnetic field configuration was $R_{ax} = 92.1$ cm and $B_t = 0.88$ T.

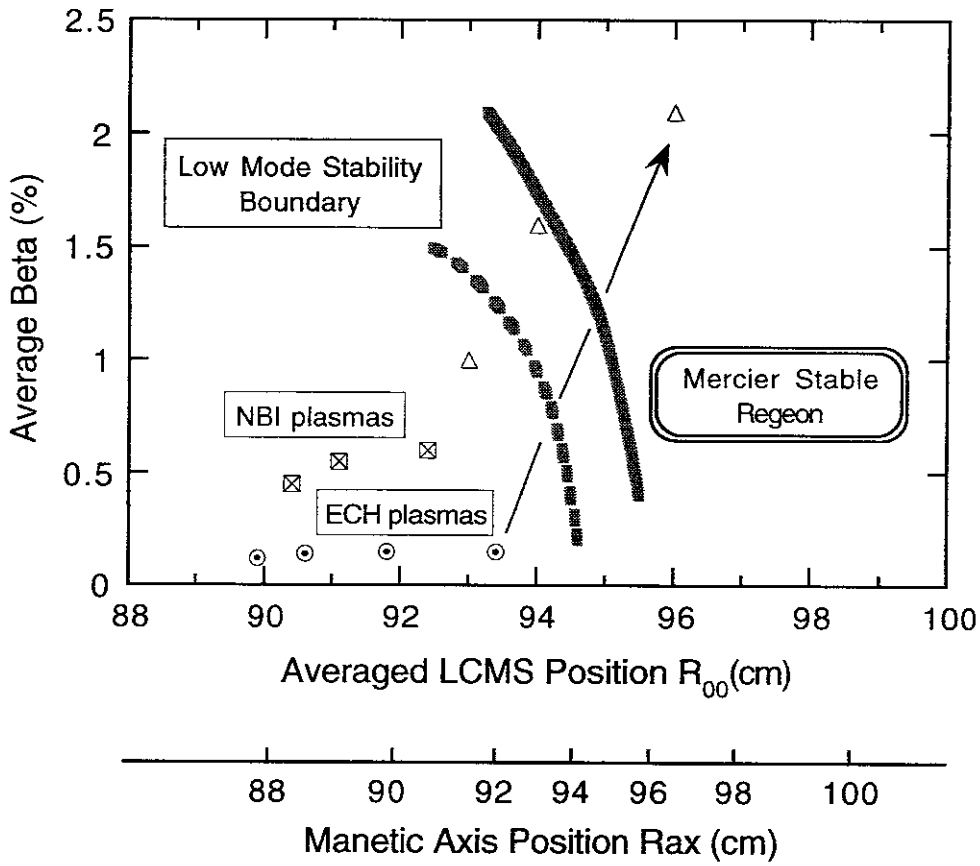

Fig. 10 Ideal MHD stability map for inward shifted configurations. Solid gray line gives Mercier stability boundary. Dotted one gives low-mode stability boundary. The value R_{ax} is given for the vacuum configuration.

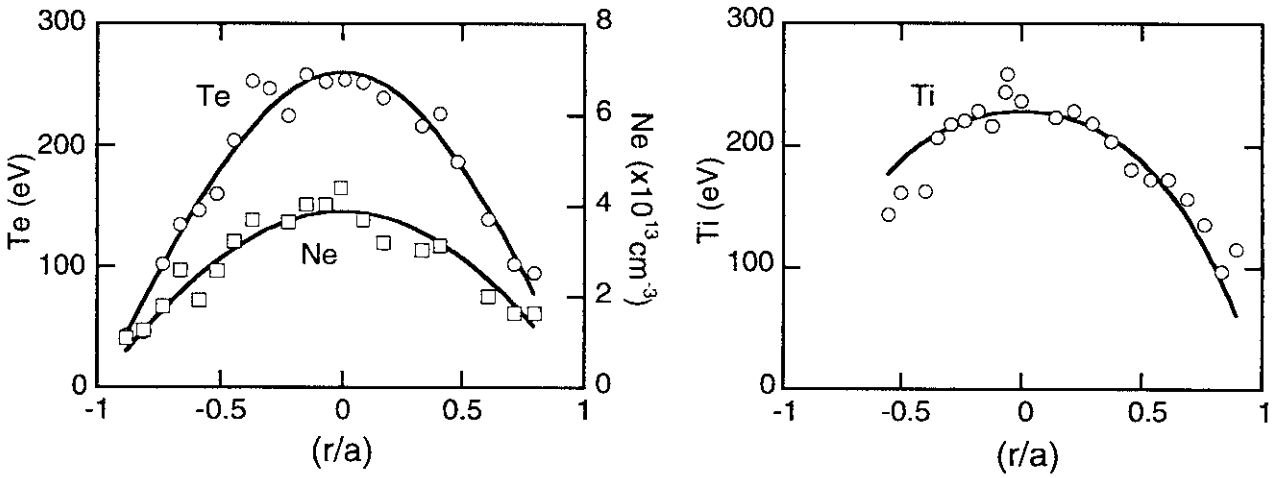

Fig.11a Plasma temperature and density profiles for standard configuration R_{ax} = 92.1 cm.

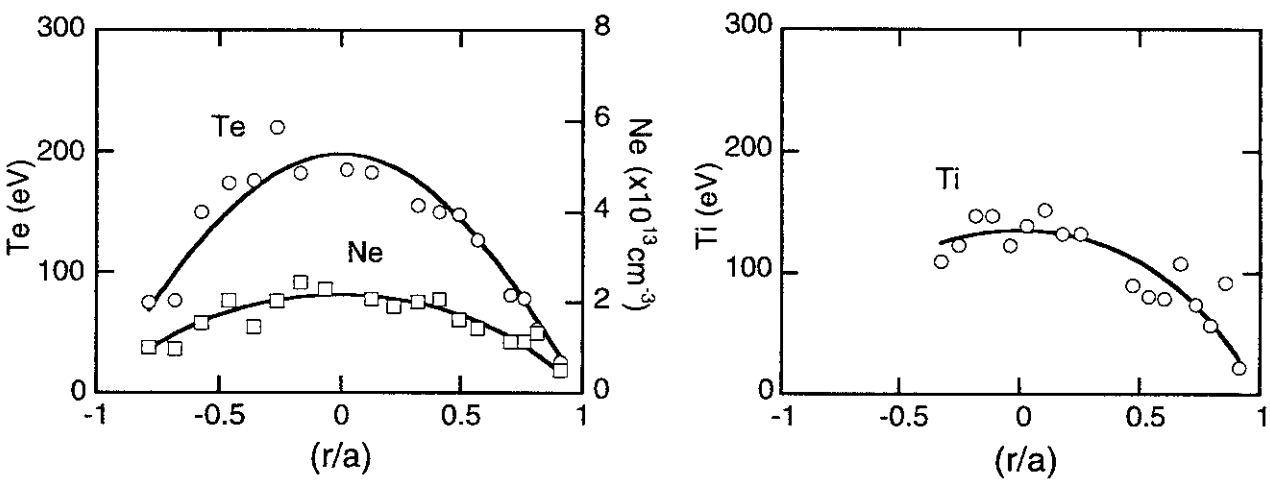

Fig.11b Plasma temperature and density profiles for drift-orbit-optimized configuration R_{ax} = 87.7 cm.

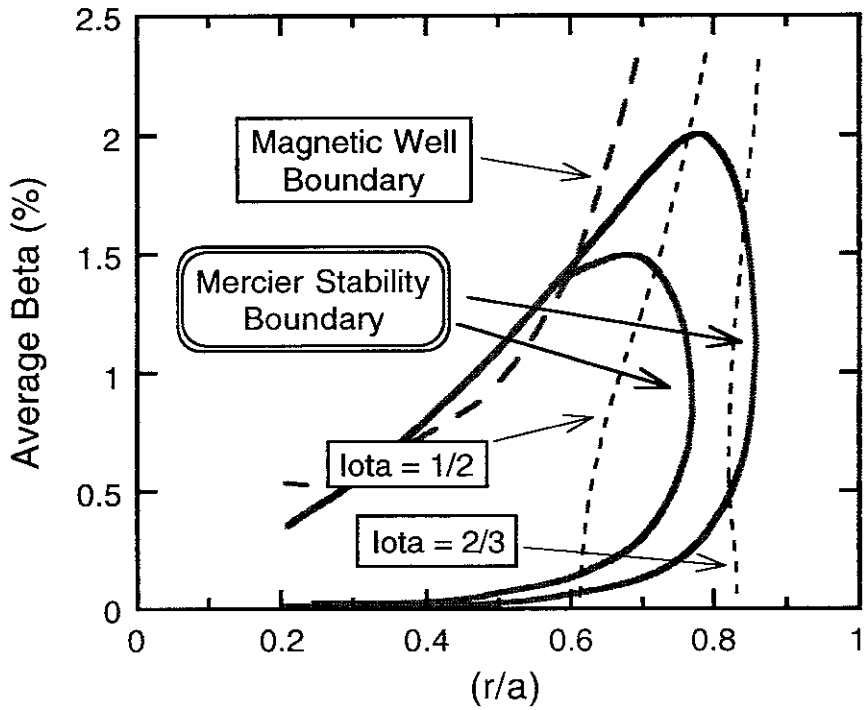

Fig. 12 Mercier stability map for R_{ax} = 88.8 cm cofiguration. Contour lines for $D_I = 0$ (larger area) and $D_I = 0.2$ (smaller area) are shown. The radius of magnetic well boundary and two low mode rational surfaces are also shown.

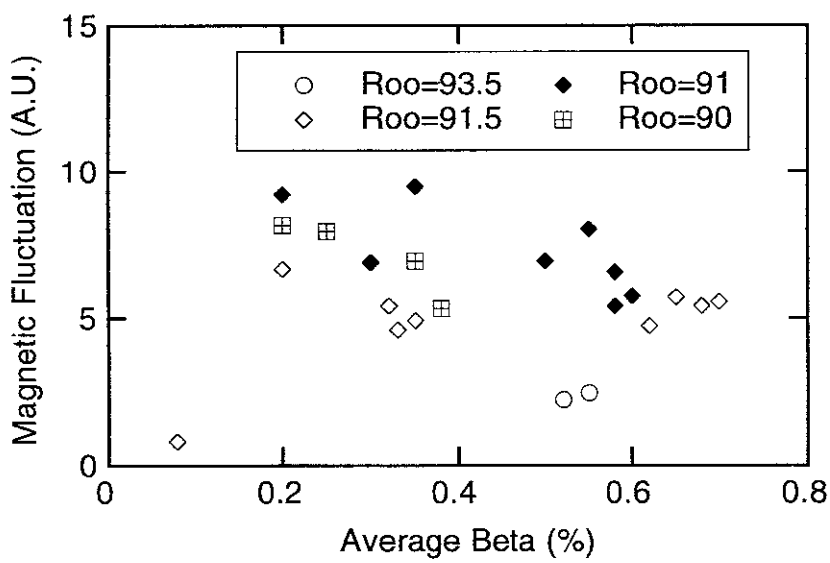

Fig. 13 Dependence of magnetic fluctuations on average beta for different LCMS positions.

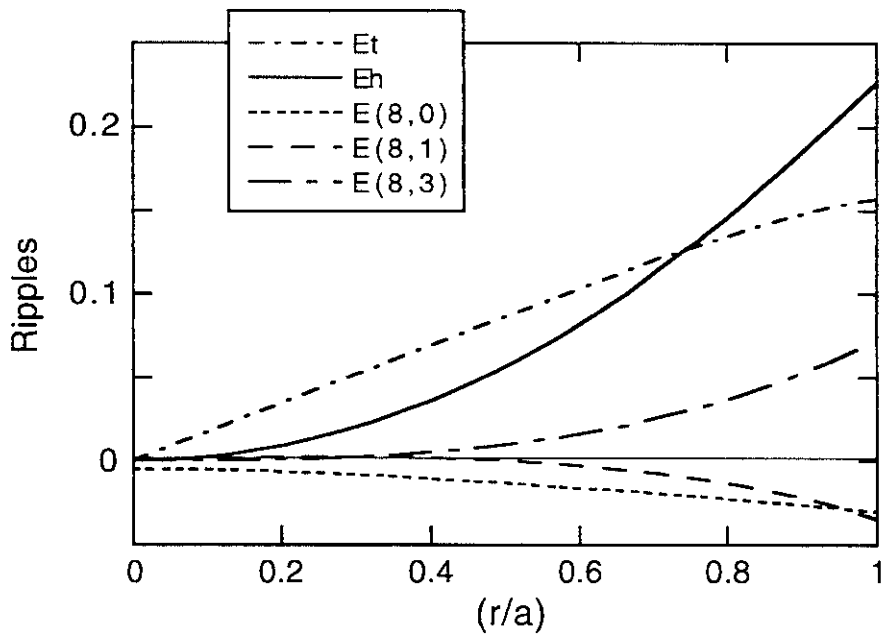

Fig. 14a Profile of magnetic field ripple structure for standard configuration R_{ax} = 92.1 cm. Selected components are Et : toroidicity, Eh : helical ripple (8, 2), mirror ripple (8, 0), side bands (8, 1) and (8, 3).

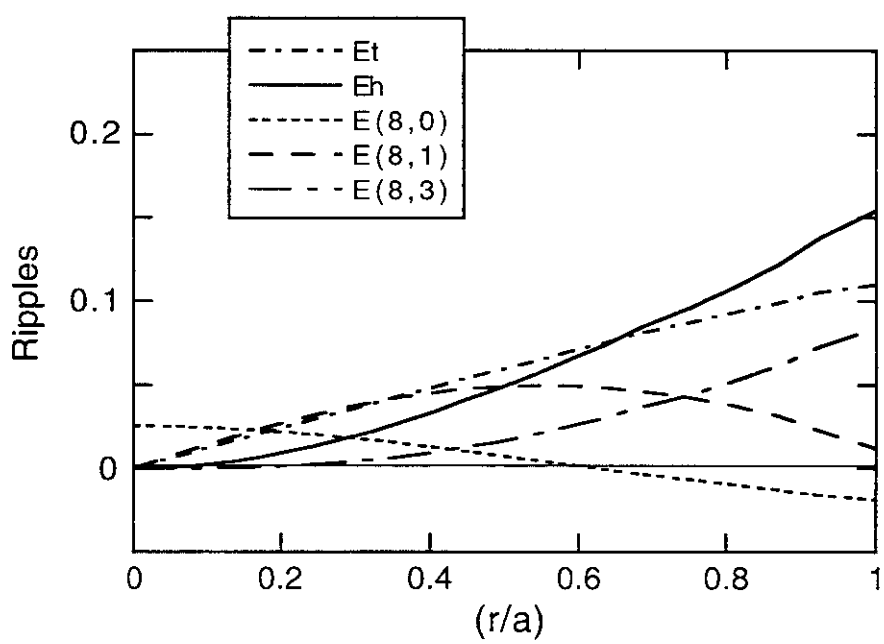

Fig. 14b Profile of magnetic field ripple structure for drift-orbit-optiminzed configuration R_{ax} = 87.7 cm.

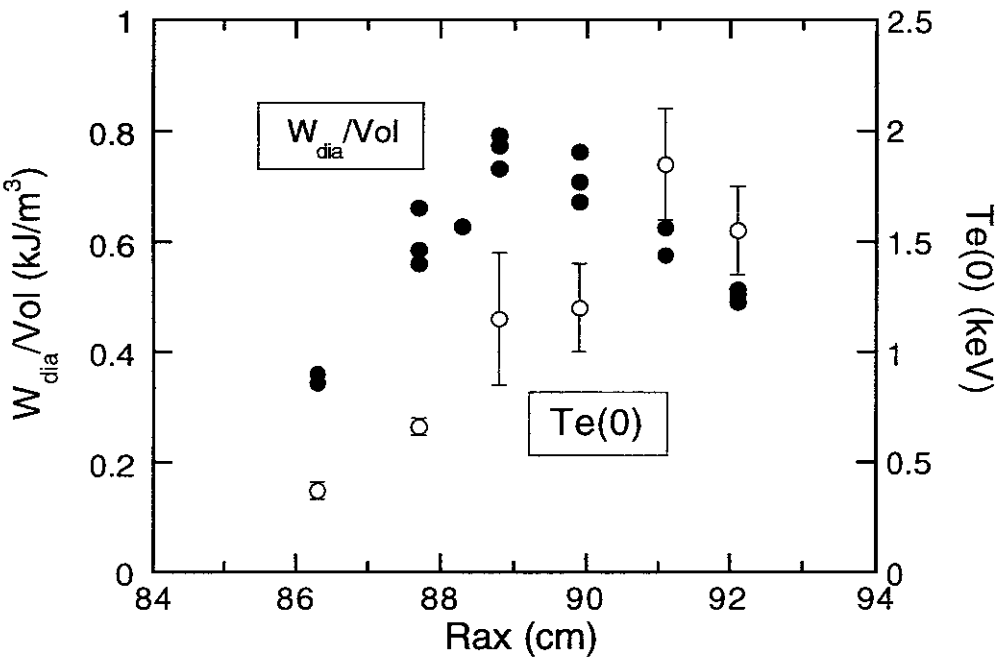

Fig. 15 Dependence of volume normalized energy and central electron temperature on the position of magnetic axis R_{ax}.

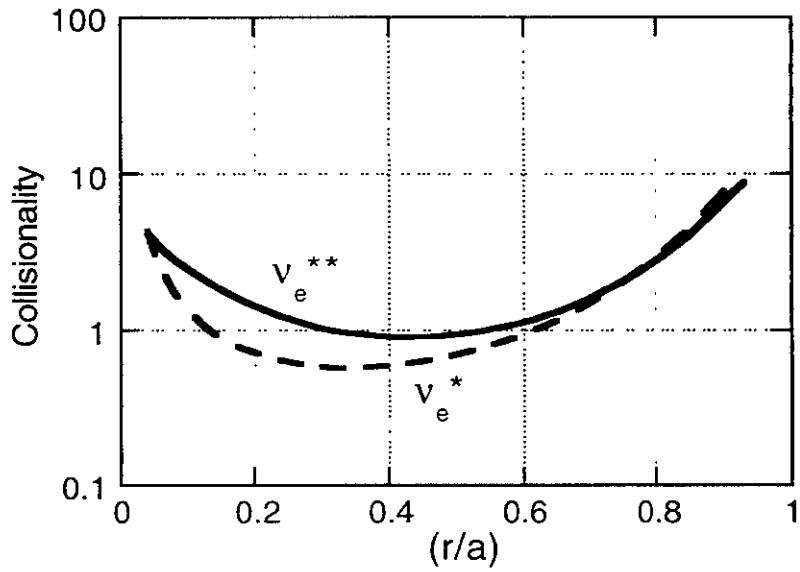

Fig. 16a Collisionality for toroidal banana particles (ν_e^*) and helical banana particles (ν_e^{**}) for ECH plasma shown in standard configuration R_{ax} = 92.1 cm at B_t = 0.88 T.

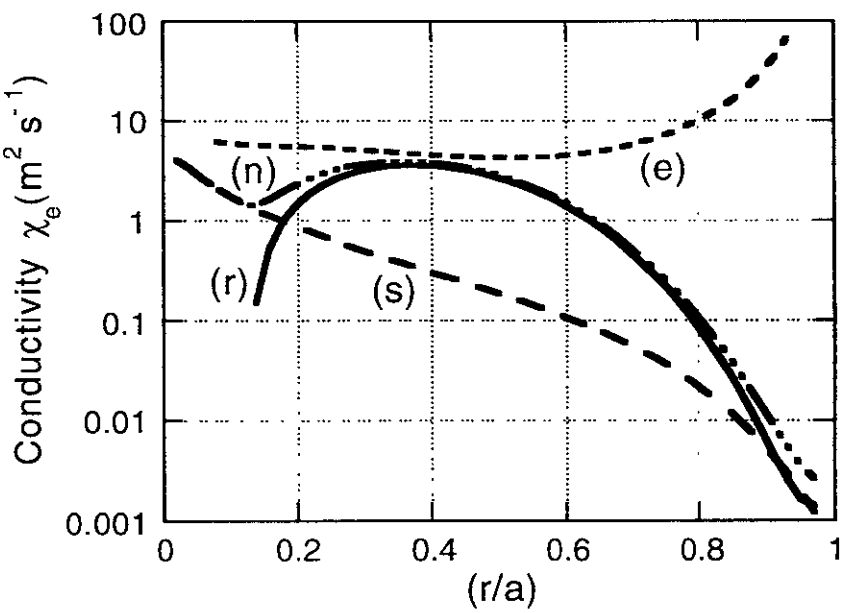

Fig.16b Neo-classical conductivities of tokamak-like symmetric term (s), helical ripple term (r) and sum of these (n) are plotted for the plasma shown in Fig. 15 at R_{ax} = 92.1 cm. Conductivity calculated from the electron temperature profile is plotted as (e). Single helicity model is used. Effect of electric field is not included.

Recent Issues of NIFS Series

NIFS-536 Lj R Hadzievski, M M Skoric, M Kono and T. Sato,
Simulation of Weak and Strong Langmuir Collapse Regimes, Jan 1998

NIFS-537 H. Sugama, W. Horton,
Nonlinear Electromagnetic Gyrokinetic Equation for Plasmas with Large Mean Flows, Feb 1998

NIFS-538 H. Iguchi, T.P. Crowley, A. Fujisawa, S Lee, K Tanaka, T Minami, S. Nishimura, K. Ida, R. Akiyama, Y. Hamada, H , Idei. M Isobe, M. Kojima, S Kubo, S Monta, S Ohdachi, S Okamura, M Osakabe, K. Matsuoka, C Takahashi and K. Toi,
Space Potential Fluctuations during MHD Activities in the Compact Helical System (CHS); Feb 1998

NIFS-539 Takashi Yabe and Yan Zhang,
Effect of Ambient Gas on Three-Dimensional Breakup in Coronet Formation Process, Feb. 1998

NIFS-540 H. Nakamura, K. Ikeda and S. Yamaguchi,
Transport Coefficients of InSb in a Strong Magnetic Field; Feb. 1998

NIFS-541 J Uramoto,
Development of ν_μ Beam Detector and Large Area ν_μ Beam Source by H_2 Gas Discharge (I); Mar 1998

NIFS-542 J. Uramoto,
Development of $bar\{\nu\}_\mu$ Beam Detector and Large Area $bar\{\nu\}_\mu$ Beam Source by H_2 Gas Discharge (II); Mar. 1998

NIFS-543 J. Uramoto,
Some Problems inside a Mass Analyzer for Pions Extracted from a H_2 Gas Discharge, Mar 1998

NIFS-544 J Uramoto,
Simplified ν_μ $bar\{\nu\}_\mu$ Beam Detector and ν_μ $bar\{\nu\}_\mu$ Beam Source by Interaction between an Electron Bunch and a Positive Ion Bunch; Mar 1998

NIFS-545 J. Uramoto,
Various Neutrino Beams Generated by D_2 Gas Discharge; Mar.1998

NIFS-546 R Kanno, N. Nakajima, T. Hayashi and M. Okamoto,
Computational Study of Three Dimensional Equilibria with the Bootstrap Current; Mar. 1998

NIFS-547 R. Kanno, N. Nakajima and M. Okamoto,
Electron Heat Transport in a Self-Similar Structure of Magnetic Islands; Apr 1998

NIFS-548 J.E Rice,
Simulated Impurity Transport in LHD from MIST; May 1998

NIFS-549 M.M. Skoric, T. Sato, A.M. Maluckov and M.S. Jovanovic,
On Kinetic Complexity in a Three-Wave Interaction; June 1998

NIFS-550 S. Goto and S. Kida,
Passive Saclar Spectrum in Isotropic Turbulence: Prediction by the Lagrangian Direct-interaction Approximation; June 1998

NIFS-551 T. Kuroda, H. Sugama, R. Kanno, M. Okamoto and W Horton,
Initial Value Problem of the Toroidal Ion Temperature Gradient Mode ; June 1998

NIFS-552 T. Mutoh, R. Kumazawa, T. Seki, F. Simpo, G. Nomura, T. Ido and T. Watari,
Steady State Tests of High Voltage Ceramic Feedthoughs and Co-Axial Transmission Line of ICRF Heating System for the Large Helical Device ; June 1998

NIFS-553 N. Noda, K. Tsuzuki, A. Sagara, N. Inoue, T. Muroga,
oronaization in Future Devices -Protecting Layer against Tritium and Energetic Neutrals-: July 1998

NIFS-554 S. Murakami and H. Saleem,

Electromagnetic Effects on Rippling Instability and Tokamak Edge Fluctuations; July 1998

NIFS-555 H. Nakamura, K. Ikeda and S. Yamaguchi,
Physical Model of Nernst Element; Aug. 1998

NIFS-556 H. Okumura, S. Yamaguchi, H. Nakamura, K. Ikeda and K. Sawada,
Numerical Computation of Thermoelectric and Thermomagnetic Effects; Aug. 1998

NIFS-557 T. Yasuhiko, O. Masaki, T. Katsuyoshi, O. Yoshihide, K. Osamu, A. Eiji, K. Toshikazu, A. Ryuichi and T. Masanobu,
Development of a High-Current Hydrogen-Negative Ion Source for LHD-NBI System; Aug.1998

NIFS-558 M. Tanaka, A. Yu Grosberg and T. Tanaka,
Molecular Dynamics of Structure Organization of Polyampholytes; Sep. 1998

NIFS-559 R. Horiuchi, K. Nishimura and T. Watanabe,
Kinetic Stabilization of Tilt Disruption in Field-Reversed Configurations; Sep. 1998
(IAEA-CN-69/THP1/11)

NIFS-560 S. Sudo, K. Kholopenkov, K. Matsuoka, S. Okamura, C. Takahashi, R. Akiyama, A. Fujisawa, K. Ida, H. Idei, H. Iguchi, M. Isobe, S. Kado, K. Kondo, S. Kubo, H. Kuramoto, T. Minami, S. Morita, S. Nishimura, M. Osakabe, M. Sasao, B. Peterson, K. Tanaka, K. Toi and Y. Yoshimura,
Particle Transport Study with Tracer-Encapsulated Solid Pellet Injection, Oct. 1998
(IAEA-CN-69/EXP1/18)

NIFS-561 A. Fujisawa, H. Iguchi, S. Lee, K. Tanaka, T. Minami, Y. Yoshimura, M. Osakabe, K. Matsuoka, S. Okamura, H. Idei, S Kubo, S. Ohdachi, S. Morita, R. Akiyama, K. Toi, H. Sanuki, K. Itoh, K. Ida, A. Shimizu, S. Takagi, C. Takahashi, M. Kojima, S. Hidekuma, S. Nishimura, M. Isobe, A. Ejiri, N. Inoue, R. Sakamoto, Y. Hamada and M. Fujiwara,
Dynamic Behavior Associated with Electric Field Transitions in CHS Heliotron/Torsatron; Oct 1998
(IAEA-CN-69/EX5/1)

NIFS-562 S. Yoshikawa,
Next Generation Toroidal Devices; Oct. 1998

NIFS-563 Y. Todo and T Sato,
Kinetic-Magnetohydrodynamic Simulation Study of Fast Ions and Toroidal Alfvén Eigenmodes; Oct 1998
(IAEA-CN-69/THP2/22)

NIFS-564 T. Watari, T. Shimozuma, Y. Takeiri, R. Kumazawa, T. Mutoh, M. Sato, O. Kaneko, K. Ohkubo, S. Kubo, H. Idei, Y. Oka, M. Osakabe, T. Seki, K. Tsumori, Y. Yoshimura, R. Akiyama, T. Kawamoto, S. Kobayashi, F. Shimpo, Y. Takita, E. Asano, S. Itoh, G. Nomura, T. Ido, M. Hamabe, M. Fujiwara, A. Iiyoshi, S. Morimoto, T. Bigelow and Y.P. Zhao,
Steady State Heating Technology Development for LHD; Oct. 1998
(IAEA-CN-69/FTP/21)

NIFS-565 A. Sagara, K.Y. Watanabe, K. Yamazaki, O. Motojima, M. Fujiwara, O. Mitarai, S. Imagawa, H. Yamanishi, H. Chikaraishi, A. Kohyama, H. Matsui, T. Muroga, T. Noda, N. Ohyabu, T. Satow, A.A. Shishkin, S Tanaka, T. Terai and T. Uda,
LHD-Type Compact Helical Reactors; Oct. 1998
(IAEA-CN-69/FTP/03(R)

NIFS-566 N. Nakajima, J. Chen, K. Ichiguchi and M. Okamoto,
Global Mode Analysis of Ideal MHD Modes in L=2 Heliotron/Torsatron Systems; Oct. 1998
(IAEA-CN-69/THP1/08)

NIFS-567 K. Ida, M. Osakabe, K. Tanaka, T. Minami, S. Nishimura, S. Okamura, A. Fujisawa, Y. Yoshimura, S. Kubo, R. Akiyama, D.S.Darrow, H. Idei, H. Iguchi, M. Isobe, S Kado, T. Kondo, S. Lee, K. Matsuoka, S. Morita, I. Nomura, S. Ohdachi, M. Sasao, A. Shimizu, K. Tumori, S. Takayama, M. Takechi, S. Takagi, C. Takahashi, K. Toi and T. Watari,
Transition from L Mode to High Ion Temperature Mode in CHS Heliotron/Torsatron Plasmas; Oct. 1998
(IAEA-CN-69/EX2/2)

NIFS-568 S. Okamura, K. Matsuoka, R. Akiyama, D.S. Darrow, A. Ejiri, A. Fujisawa, M. Fujiwara, M. Goto, K. Ida H. Idei, H. Iguchi, N. Inoue, M. Isobe, K. Itoh, S. Kado, K. Kholopenkov, T. Kondo, S. Kubo, A. Lazaros, S. Lee, G. Matsunaga, T. Minami, S. Morita, S. Murakami, N. Nakajima, N. Nikai, S. Nishimura, I. Nomura, S. Ohdachi, K. Ohkuni, M. Osakabe, R. Pavlichenko, B. Peterson, R. Sakamoto, H. Sanuki, M. Sasao, A. Shimizu, Y. Shirai, S. Sudo, S. Takagi, C. Takahashi, S. Takayama, M. Takechi, K. Tanaka, K. Toi, K. Yamazaki, Y. Yoshimura and T. Watari,
Confinement Physics Study in a Small Low-Aspect-Ratio Helical Device CHS; Oct. 1998
(IAEA-CN-69/OV4/5)